ELSEVIER

Atmospheric Research 72 (2004) 39–56

ATMOSPHERIC RESEARCH

www.elsevier.com/locate/atmos

A self-sufficient approach for GERB cloudy radiance detection

V. Cuomo[a], C. Filizzola[b], N. Pergola[a], C. Pietrapertosa[a], V. Tramutoli[b,*]

[a] *Institute of Methodology for Environmental Analysis, Tito Scalo (PZ), Italy*
[b] *University of Basilicata, Potenza, Italy*

Received 1 August 2003; received in revised form 23 February 2004; accepted 31 March 2004

Abstract

Geostationary Earth Radiation Budget (GERB) is the broadband radiometer onboard the Meteosat Second Generation (MSG) platform, launched at the end of August 2002 and still in commissioning phase. GERB data is planned to be used in many applications concerning Earth Radiation Budget (ERB) calculation. In order to evaluate the impact of clouds on ERB, a cloud detection is required and, at present, a cloud mask based on higher spatial and spectral resolution data acquired by Spinning Enhanced Visible and Infrared Imager (SEVIRI), the imager onboard the same MSG platform, is planned to be used in order to identify cloudy GERB soundings.

As an alternative, a self-sufficient (only based on GERB data) method (OCA, the One-channel Cloudy-radiance-detection Approach) is proposed, as a time-saving and, probably, more suitable solution than the planned co-location approach.

In this paper, preliminary results obtained by using several years of Meteosat data as well as GERB synthetic radiances (produced from Meteosat-7 observations) are presented. It is shown how results obtained by using GERB data alone can be comparable (and better in terms of number and spatial distribution of clear-sky GERB soundings identified) to the ones achieved if the co-location of a higher resolution cloud mask is used.

Keywords: Cloudy radiance mask; Dynamic thresholds; GERB; SEVIRI

* Corresponding author. Dipartimento di Ingegneria e Fisica dell' Ambiente, DIFA-Università degli Studi della Basilicata, Campus Macchia Romano, 85100 Potenza, Italy. Tel.: +39-971-205205; fax: +39-971-205160.
E-mail address: tramutoli@unibas.it (V. Tramutoli).

0169-8095/$ - see front matter © 2004 Elsevier B.V. All rights reserved.
doi:10.1016/j.atmosres.2004.03.030

1. Introduction

For all satellite applications devoted to the retrieval of Earth atmosphere and surface parameters, cloud detection is a fundamental step. In fact, clouds prevent the retrieval of both surface and atmospheric parameters as far as optical spectral bands are used. Even in the case that clouds themselves are the object of study, cloud identification is required, in order to know where clouds are present and extract information concerning their properties (temperature at the top, reflectance, optical thickness, etc.). The cloud flag information is known to be very important, also for the climatology community, in the derivation of average (e.g. monthly) clear-sky albedo and clear-sky thermal flux by removing data contaminated by clouds.

Whatever is the application, radiances which reach a satellite sensor can turn out to be modified by the presence of clouds according to their features (optical thickness, ice/water content, temperature of the top, height, size, etc.), the spectral band of observation and cloud thickness and/or fraction within the Instantaneous Field Of View (IFOV).

Proposed algorithms for cloud detection (see, for instance, Ackerman et al., 1998; Arking and Childs, 1985; Coakley and Bretherton, 1982) are traditionally based on cloud spectral properties (typically higher VIS–NIR reflectance and lower TIR brightness temperature), which allow us to distinguish clouds from underlying terrestrial surface. Multi-channel sensors give the opportunity to exploit the different spectral features of clouds at different wavelengths, so that *multi-spectral approaches* can be applied in order to identify clouds and produce, finally, a *cloud mask*. Multi-spectral algorithms (e.g. Saunders, 1986; Saunders and Kriebel, 1988; Derrien et al., 1993) are usually based on fixed-threshold tests on multi-spectral satellite radiances (or their combinations) which work well for some cloud types or climate regions (wherever there is a strong contrast between clouds and surface), but, as the authors themselves recognize, they may give poor results for situations of low contrast (low-lying clouds, thin cirrus, broken clouds, sea ice, snow-covered land, etc.). Particularly poor results may be achieved when such algorithms are applied to the global scale mainly because of the high space–time variability of atmospheric and surface parameters, whose knowledge (particularly over land) is usually lacking or insufficient. Moreover, fixed threshold methods, developed for a specific sensor, turn out not to be immediately exportable to different satellite sensors.

Whether such limitations are considered or not, multi-spectral approaches cannot be directly used on sensors with low spectral capabilities. In these cases, data acquired by high spatial/spectral resolution sensors, aboard the same platform, is processed in order to obtain an independent cloud mask based on traditional multi-spectral algorithms. The resulting cloud mask is, then, co-located on the lower resolution sensor image.

This is the case of GERB, a radiometer with only two broad bands, presently in the commissioning phase, on board the new Meteosat Second Generation platform (MSG). For such an instrument, it is planned to rely upon Spinning Enhanced Visible and Infrared Imager (SEVIRI), which is the multi-spectral sensor aboard the same bus.

Cloud mask co-location is a time-consuming process because different resolution data is not generally taken either at the same time or at the same space position: in the GERB case, data is acquired every 5 min with a spatial resolution of about 50 km, while with SEVIRI, data is acquired every 15 min with a spatial resolution of 3 km.

In order to be detectable, radiance variations produced by clouds entering an instrument IFOV have to be larger than the variations normally observed in clear-sky conditions. Nevertheless, the variability caused by a cloud can result as low as (or lower than) natural variability because of cloud and/or instrumental characteristics. For example, semi-transparent clouds can alter radiances just as natural variations of atmospheric parameters can, or an IFOV, which is larger than cloud size, could not record cloud presence. Consequently, clouds are only detectable whenever they alter the observed radiances by more than the normal variability of clear-sky values. For this reason, whenever clouds within the IFOV have no influence on the radiance which reaches the sensor, such an IFOV turns out to be practically indistinguishable from a clear-sky one. Traditional multi-spectral cloud detection methods operate with a cascade of tests at the end of which an image pixel can be flagged as cloudy even if only one spectral band (or band combination) exhibits a radiance significantly diverging from the one expected in clear sky conditions. For this reason, resulting cloud masks do not reveal to what extent single spectral bands are affected by the presence of clouds. In this way, such cloud mask products are biased to a high amount of clouds protecting however their reliability to clear-sky condition detection. When a broadband sensor (like GERB) is used for applications (like ERB studies) which only need to know if the radiance collected by the sensor within a specific spectral band is affected or not by clouds, information coming from higher resolution co-located products (like SEVIRI-based cloud masks) may not be strictly necessary, or even misleading.

For instance, the proposed use of co-located, SEVIRI-based cloud mask (about 300 soundings within a single GERB IFOV) to identify cloudy GERB soundings, is to be expected to introduce, at least, the following additional problems:

(a) the SEVIRI derived cloud masks, $CM_S(i,j)$ giving for each GERB IFOV (at GERB image coordinates i,j) the fraction of cloudy SEVIRI soundings within it, could have no relation with real deviations from clear-sky values of GERB radiances measured in a specific GERB band. Being based on tests performed on spectral bands completely different from the GERB ones, SEVIRI-based cloud masks are obviously biased to a high amount of clouds.
(b) this bias is further increased if we consider that not only spectral bands but also the spatial resolution of SEVIRI and GERB are very different. Several studies (see for instance, Cuomo et al., 1997; Tramutoli et al., 1998) have already demonstrated how the interchange of products achieved by satellite packages having different spectral and spatial capabilities can be profitably done only after well-controlled inter-calibration procedures (that very rarely reduce to simple co-location and/or averaging processes) whose rationale and effectiveness is strictly related to the specific application. For instance, assuming as cloud-free only GERB soundings having $CM(i,j)=0$ surely better protects from introducing undesired cloud contaminated radiances in the following GERB data processing steps. This choice, however, due to the very coarse GERB spatial resolution, will drastically reduce the population of available clear-sky GERB soundings across the scene. To establish a higher CM_{MAX} upper limit for clear-sky GERB sounding identification (in order to increase the population of clear-sky soundings) is a very hazardous task when, as in our case, only

the fractional cloud coverage within a GERB IFOV is considered without information on its real effect on GERB radiances (which, instead, can be highly variable depending on cloud characteristics and specific observational spectral band). The objective of identifying all clear-sky GERB soundings avoiding to mistake partly cloudy for clear-sky GERB soundings, is then, in principle, not achievable by operating whatever choice of CM_{MAX} on a SEVIRI-based cloud mask. In any case, even considering the information on spatial distribution (not on radiative properties) of meteorological clouds sufficient for a GERB cloud mask construction, the choice of a suitable CM_{MAX} limit remains not a negligible issue as it was demonstrated by several studies (Cuomo et al., 1993; Serio and Tramutoli, 1995; Pietrapertosa et al., 2001a) showing how sensitive to this choice is the number (and the spatial distribution) of clear-sky soundings identifiable across a scene. As we will see, depending on the specific application, such a circumstance could have more or less important effects.

(c) For most ERB products expected from GERB, a homogeneous spatial distribution of cloud-free soundings across the scene is particularly desirable. One of the most important climatological product expected by GERB is, for instance, the estimate of cloud radiative forcing (CRF). Its accuracy is mainly related to our present capability of retrieving *cloud-cleared* GERB radiances (i.e. the ones we would measure in the absence of clouds) at each GERB IFOV previously identified as affected by clouds. Cloud-cleared radiances at cloudy locations are usually determined on the basis of the remaining, previously identified, clear-sky soundings (see, for instance, Rizzi et al., 1994). The more and better spatially distributed across the scene, they will be, the better the reconstruction of the cloud-cleared image (Cuomo et al., 1999). To this aim a single, spatially isolated clear-sky sounding, within a cloudy portion of the scene, can permit us to improve the cloud-clearing process much more than hundreds in a largely clear portion of the scene. The use of a SEVIRI-based cloud detection mask, biased to a high amount of clouds, is then particularly detrimental to this kind of application.

It should be clear now that detecting the presence of a cloud within a sounder's IFOV and identifying as cloudy-affected the radiance measured in a specific spectral band can be quite different tasks whose differences becomes particularly evident in the case of the SEVIRI–GERB coupling. As we will see, for sounders like GERB a self-sufficient *cloudy radiance mask* (indicating, for a *specific* band of observation, where measured radiances are affected by a cloud) rather than an imported *cloud mask* (indicating where clouds are, independently of their effects on the radiance measured in a specific band) can often represent the most suitable solution.

A *cloudy radiance* detection scheme (OCA, One-channel Cloudy-radiance-detection Approach) has been suggested (Tramutoli, 1998) and preliminarily tested (Tramutoli et al., 2000; Pietrapertosa et al., 2001b) which seems to permit a self-sufficient (i.e. based only on satellite data at hand) identification of cloudy radiances even for satellite packages having (like GERB) very low (up to the limit of only one spectral band) multi-spectral capabilities.

In this paper, the OCA scheme will be described (even in comparison with some existing *cloud-detection* method) and results achieved after its application to several years

of Meteosat and GERB synthetic data (derived from real Meteosat observations) will be presented.

2. The OCA approach

Like other methods, the OCA scheme considers cloudy (i.e. affected by clouds) those satellite radiances which significantly differ from those expected in clear sky conditions. Hence, differences regard:

(a) how expected clear-sky radiances are defined.
(b) how the right thresholds are chosen or on which basis the difference from measured radiance and its expected clear-sky radiance value is classified as "significant" and then attributed to the presence of a cloud (and NOT to a normal variation of the clear-sky radiance).

As we will see, and differently from most of the quoted fixed-threshold approach, OCA is conceived to automatically produce both clear-sky radiances and tuneable thresholds for cloudy radiance detection, which are specific for each image location and time of observation. No ancillary data is required (e.g. radiative transfer model, climatological data, land cover information, etc.) nor the ones achievable from other spectral bands of the same instrument (self-sufficiency). Its exportability on whatever geographic area and satellite package is straightforward, requiring no specific scheme change.

The general OCA scheme can be resumed in the following three steps.

2.1. Data pre-processing

A historical data set of navigated and co-located satellite imagery is selected in order to be as homogeneous (same platform, same time of day, same month of the year, etc.) as possible to the image to be processed for detection.

Each element of such a data set, representing the satellite radiance $R_\lambda(\boldsymbol{r},t)$ measured in spectral band λ at time $t\in T$, at a pixel centered at coordinates $\boldsymbol{r}\in D$, is considered as a realisation of a space–time process defined on a $D \times T$ *space–time domain* (being $D\in\mathcal{R}^2$ the square lattice of sites $\boldsymbol{r}\in D$ where values of $R_\lambda(\boldsymbol{r},t)$ are available or simply represented and $T\in$R the collection of N *temporal sites* ($T\equiv\{t_1,t_2,..,t_N\}$) for which the values of $R_\lambda(\boldsymbol{r},t)$ are available). At each fixed time t', $R_\lambda(\boldsymbol{r},t')$ represents a realization of a purely spatial process (image), for each fixed location $\boldsymbol{r}'$, $R_\lambda(\boldsymbol{r}',t)$ represents a realization of a time-series process.

2.2. Computing reference fields for clear-sky radiances

By using the homogeneous historical records selected in the previous step and for each time-series $R_\lambda(\boldsymbol{r}',t)$, the time average $\mu_R(\boldsymbol{r}')$ and the standard deviation $\sigma_R(\boldsymbol{r}')$ are computed producing two reference image $\mu_R(\boldsymbol{r})$ and $\sigma_R(\boldsymbol{r})$.

In order to avoid that, in mostly cloudy conditions, cloudy radiances dominate the averaging process, a preliminary iterative 2σ-clipping[1] procedure (primed by a drastic entry threshold) is applied to eliminate from each $R_\lambda(\boldsymbol{r}',t)$ time-series, radiances related to too cold (if thermal infrared channels are used) or too reflecting (if visible channels are considered) image pixels. Reference images $\mu_R(\boldsymbol{r})$ and $\sigma_R(\boldsymbol{r})$ are then computed only on the time-series elements which have survived at the end of such a clipping procedure.

2.3. Cloudy radiance detection

The last step is the computation pixel-by-pixel, for the image at hand, of the $\otimes_R(\boldsymbol{r},t)$ index, which is defined as follows:

$$\otimes_R(\boldsymbol{r},t) = \frac{[R_\lambda(\boldsymbol{r},t) - \mu_R(\boldsymbol{r})]}{\sigma_R(\boldsymbol{r})}$$

being $R_\lambda(\boldsymbol{r},t)$ the signal measured (at location $\boldsymbol{r}$ and time t, in spectral band λ), $\mu_R(\boldsymbol{r})$ the mean and $\sigma_R(\boldsymbol{r})$ the standard deviation computed in the previous step.

$\otimes_R(\boldsymbol{r},t)$ index gives, for each image pixels, an estimate of the difference between measured radiance $R_\lambda(\boldsymbol{r},t)$ and its expected clear-sky value $\mu_R(\boldsymbol{r})$, weighted by the normal variability of clear-sky radiance as historically observed at the same place in similar observational conditions. Measured satellite radiances are expected to be more affected by clouds as higher $\otimes_R(\boldsymbol{r},t)$ is in absolute value. In particular, higher positive $\otimes_R(\boldsymbol{r},t)$ values (negative values) are expected for cloudy radiances as far as visible (thermal infrared) $R_\lambda(\boldsymbol{r},t)$ radiances are considered.

On this basis, and for each considered spectral band, OCA allows us to identify cloud-contaminated radiances contemporarily giving, by $\otimes_R(\boldsymbol{r},t)$ index values, the statistical significance of such a contamination.

The use of such an approach (and indices like $\otimes_R(\boldsymbol{r},t)$) is quite usual in climate studies but very rarely, and only in the last decade (e.g. Gutman et al., 1996), it has been extended to satellite observations and, more recently (Tramutoli, 1998), to natural (Pergola et al., 1998, 2001, 2004; Tramutoli et al., 2001a,b; Di Bello et al., 2004; Filizzola et al., 2004) and environmental (Lasaponara et al., 1998; Cuomo et al., 2001) hazard monitoring. Such an extension is by no means trivial because of the variability of observation conditions which strongly affect space–time behaviour of measured radiances and makes it hard to apply conventional statistical models to time-series of satellite records. Specific strategies are then required (often different depending on the application) in order to reduce these spurious contributions (in part listed in Gutman et al., 1996) to satellite radiances time-

[1] $k\sigma$-clipping is a quite standard statistics method which iteratively updates the population of a time-series $R(t)$ (with mean μ_R and standard deviation σ_R) saving for further processing only those time-series elements having $|R(t) - \mu_R| < k\sigma_R$ (symmetric clipping). At each new step, new μ_R and σ_R values are computed on the time-series elements survived to the previous $k\sigma$-clipping step. The process converges when $k\sigma$-clipping produces no further elimination. Asymmetric clipping has been used in our case, using the surviving condition $R(t) - \mu_R < 2\sigma_R$ for visible radiances and $R(t) - \mu_R > -2\sigma_R$ for infrared ones.

series including, for instance, refined geo-referencing and co-location procedures (e.g. Pergola and Tramutoli, 2000, 2003).

An example of an application-dedicated algorithm is MASCI[2] which was proposed by Gutman et al. (1994) for reducing cloud contamination in GVI[3] products obtained from time-series of NOAA/AVHRR imagery. Like OCA, also the MASCI scheme is based on a preliminary characterization of the clear-sky radiance field, in terms of temporal means and standard deviations, which are computed for each location and time of observation. The method used in MASCI to build such clear-sky radiance reference fields is, instead, very different making such a method applicable only on vegetated areas and not, as the authors themselves underline, over snow covered and desert areas or on the sea. Moreover, requiring TIR, VIS and NIR radiances MASCI is not applicable to satellite packages without those spectral capabilities and, in general, to night-time satellite images. By contrast OCA is, in principle, at the same time generally applicable (wherever and on whatever satellite package) and remains, for each instrument spectral band, self-sufficient (no ancillary data or multi-spectral capabilities are required).

Some similarity with the OCA concept exhibits also the ISCCP[4] (Rossow and Garder, 1993) cloud-detection approach. Like OCA, ISCCP is based on place/time specific clear-sky radiance fields computed at each place on the basis of the analysis of images collected from 5 to 30 days before. Nevertheless, the OCA approach is different from ISCCP from many points of view. OCA, unlike ISCCP, is really based on dynamical thresholds as even the "...uncertainty in the clear values..." (Rossow and Garder, 1993) is dynamically and automatically determined, pixel-by-pixel, on the basis of the standard deviation reference fields. Such an uncertainty cannot be considered constant (or simply parameterised as in ISCCP) either on large areas or for all seasons. Moreover, being computed (pixel-by-pixel) on the basis of satellite records acquired during several years (same month), the OCA clear sky reference images $\mu_R(\boldsymbol{r})$ and $\sigma_R(\boldsymbol{r})$ turn out to be much less affected by persistent cloud coverage.

Finally OCA, unlike ISCCP, does not need to know a priori where snow, ice,..., are; it does not need ancillary data, then being really self-sufficient also from this point of view.

CLAVR[5]-3 (Vemury et al., 2001), the NOAA/NESDIS procedure developed for AVHRR in order to better define pixels flagged "uncertain" by the fixed threshold cloud detection method CLAVR-1 (Stowe et al., 1991, 1999), is another technique OCA can resemble. Like OCA, CLAVR-3 is based on dynamical thresholds (in this case based on imagery acquired from 6 to 10 days before) but, like ISCCP, it is poorly reliable in the case of persistent cloud coverage and, like MASCI, requires ancillary information (e.g. NDVI[6]) which makes this method not self-sufficient and applicable only during the daytime.

[2] Multispectral Algorithm for Screening Composite Imagery (MASCI).

[3] Global Vegetation Index (GVI) determined on the basis of the satellite radiances measured in the visible and near-infrared spectral range.

[4] International Satellite Cloud Climatology Project.

[5] Cloud from AVHRR.

[6] Normalized Differential Vegetation Index determined on the basis of the satellite radiances measured in the visible and near-infrared spectral range.

OCA's $\otimes_R(\boldsymbol{r},t)$ index can be considered *intrinsically robust* (according to Cressie's, 1993; Menke's, 1984, definitions) as it does not require (being only based on satellite data at hand) any specific assumption on data distribution neither to be made nor to be met. The OCA approach is, moreover, intrinsically exportable (to different geographic locations, seasons and instrumental packages) since it is completely based on the analysis of data at hand.

When OCA is applied to sensors onboard polar satellite platforms, signal variations related to co-location errors, view angle and time of observation changes could contribute to the increase of the local variance, reducing the corresponding $\otimes_R(\boldsymbol{r},t)$ values (in modulus) so that, in these cases, a reduced sensitivity to cloud contamination is to be expected.

3. OCA application to Meteosat data

When geostationary rather than polar satellite platforms are considered, improvements in $\otimes_R(\boldsymbol{r},t)$ sensitivity in detecting signal variation (even in the presence of a larger IFOV) are expected. In such a case, it is easy to understand that the denominator of $\otimes_R(\boldsymbol{r},t)$ tends to decrease, because local variability $\sigma(\boldsymbol{r})$ turns out to be lower mainly thanks to:

(a) the geostationary attitude which offers a better quality of the image to image superimposition together with the saving of the same angle of view for each image pixel;
(b) the improved time-resolution which will reduce both natural (lower image-to-image variability of the local signal) and observational (greater homogeneity of time-series elements) noise.

Such an expected increase in sensitivity is particularly important for low spectral (and spatial) resolution sensors, like GERB, employed in radiative budget computations.

For such sensors, OCA could effectively permit a self-sufficient cloudy radiance mask without the need to rely (with all the possible implications described in Introduction) on cloud masks imported from other satellite packages having different spatial and spectral capabilities.

Before implementing OCA on synthetic GERB data, the method has been applied to 4 years of real Meteosat[7] data in order to verify the OCA performances even by comparison with available operational products.

According to the OCA prescriptions, a set of images, collected in the same month and at the same daytime, was first selected.

For OCA implementation on Meteosat data, three data sets (each composed by about 120 Meteosat full disk images) have been considered:

(A) Summer/night time infrared channel (IR) data set: images acquired by IR channel at 24:00 GMT (slot 48), during the month of August, from 1996 to 1999.

[7] Meteosat Visible and InfraRed Imager (MVIRI) is the sensor onboard the geostationary Meteosat satellite to which, as usually done, we will refer simply as Meteosat.

(B) Autumn/daytime IR data set: images acquired by IR channel at 11:00 GMT (slot 22), during the month of October, from 1996 to 1999.
(C) Autumn/daytime visible channel (VIS) data set: images acquired by VIS channel at 11:00 GMT (slot 22), during the month of October, from 1996 to 1999.

For each of the above-mentioned data sets of Meteosat images (calibrated according to EUMETSAT standard procedure described on http://www.eumetsat.de), the temporal mean $\mu_\lambda(\boldsymbol{r})$ and the standard deviation $\sigma_\lambda(\boldsymbol{r})$ were computed at each location $\boldsymbol{r}$ of the scene. The 2σ-clipping was preliminary applied to each time-series $R_\lambda(\boldsymbol{r}',t)$ primed (see before) by a raw cut at 265 K for IR images; at 90 W/m^2/str (land) and 30 W/m^2/str (sea) for VIS images.

Fig. 1 shows the reference fields $\mu_R(\boldsymbol{r})$ and $\sigma_R(\boldsymbol{r})$ for the three Meteosat data sets considered.

It is possible to distinguish easily the areas (like equatorial strip) with higher signal variability (higher standard deviations) as well as areas with typically higher surface temperature (brighter tones over $\mu_{\mathrm{IR}}(\boldsymbol{r})$ images) or more reflecting surfaces (brighter tones over $\mu_{\mathrm{VIS}}(\boldsymbol{r})$ image) like Northern Africa.

For each pixel of the IR image at hand, the following $\otimes_{\mathrm{IR}}(\boldsymbol{r},t)$ index was computed:

$$\otimes_{\mathrm{IR}}(\boldsymbol{r},t)=\frac{[\mathrm{IR}(\boldsymbol{r},t)-\mu_{\mathrm{IR}}(\boldsymbol{r})]}{\sigma_{\mathrm{IR}}(\boldsymbol{r})}$$

For each pixel of the VIS image at hand, the following $\otimes_{\mathrm{VIS}}(\boldsymbol{r},t)$ index was computed:

$$\otimes_{\mathrm{VIS}}(\boldsymbol{r},t)=\frac{[\mathrm{VIS}(\boldsymbol{r},t)-\mu_{\mathrm{VIS}}(\boldsymbol{r})]}{\sigma_{\mathrm{VIS}}(\boldsymbol{r})}$$

Some examples of cloudy radiance masks coming from the $\otimes_R(\boldsymbol{r},t)$ computation for the three Meteosat data sets are shown in Fig. 2. For data set A (image of 1st August 1999), OCA cloudy radiance masks are presented, for different cuts ($\otimes_{\mathrm{IR}}(\boldsymbol{r},t)<-1$, -3 and -6): a stronger cut-level ($\otimes_{\mathrm{IR}}(\boldsymbol{r},t)<-6$) is more selective for cloudy-radiance selection, while a weaker cut-level ($\otimes_{\mathrm{IR}}(\boldsymbol{r},t)<-1$) is more selective for clear-radiance detection. This means that, according to the application specific requirements, OCA allows us to use different cutting levels: lower, to be sure of eliminating all the significant cloud effects or larger, to be sure to select only cloudy radiances (OCA tuneability).

In the centre and bottom of Fig. 2, cloudy radiance masks for data sets B and C, respectively, are shown for the image of 7th October 1996. Also for such data sets, different cut-levels are presented but in a compressed graphic mode.

A general look at the cloudy radiance masks for the same day (and same slot), obtained applying OCA separately to IR and VIS images (such as the ones in Fig. 2B and C), allows us to easily realize that, for detecting most clouds, infrared or visible channels can be used indifferently. Nevertheless, some clouds may mainly affect radiances in infrared rather than in visible channel (cirrus) or vice versa (boundary layer cumulus). In such cases, cirrus can be better detected as a significant signal variation with respect to the IR reference field, while low-lying clouds can be better recognized as values which

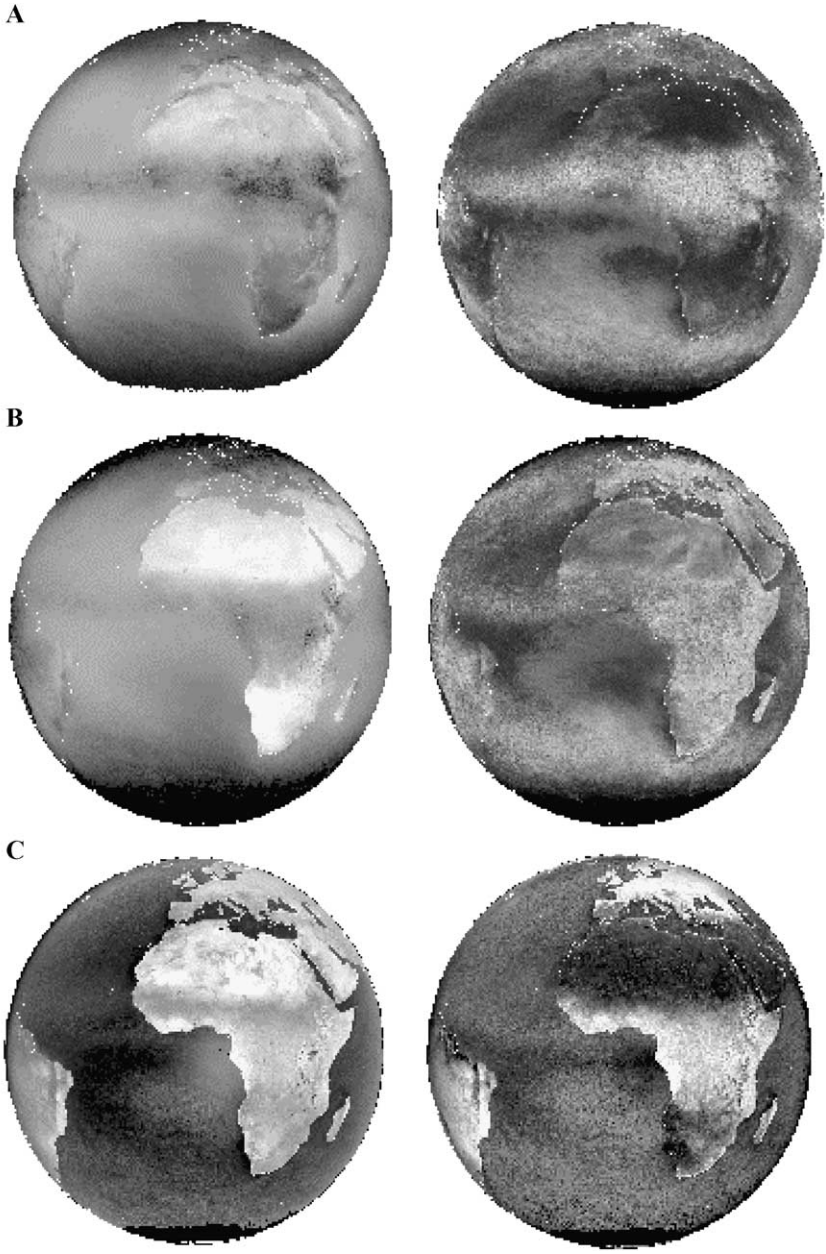

Fig. 1. Reference fields coming from Meteosat images from 1996 to 1999: mean (on the left) and standard deviation (on the right) for August—24:00 GMT—IR channel (A), October—11:00 GMT—IR channel (B), October—11:00 GMT—VIS channel (C). Brighter tones indicate higher values.

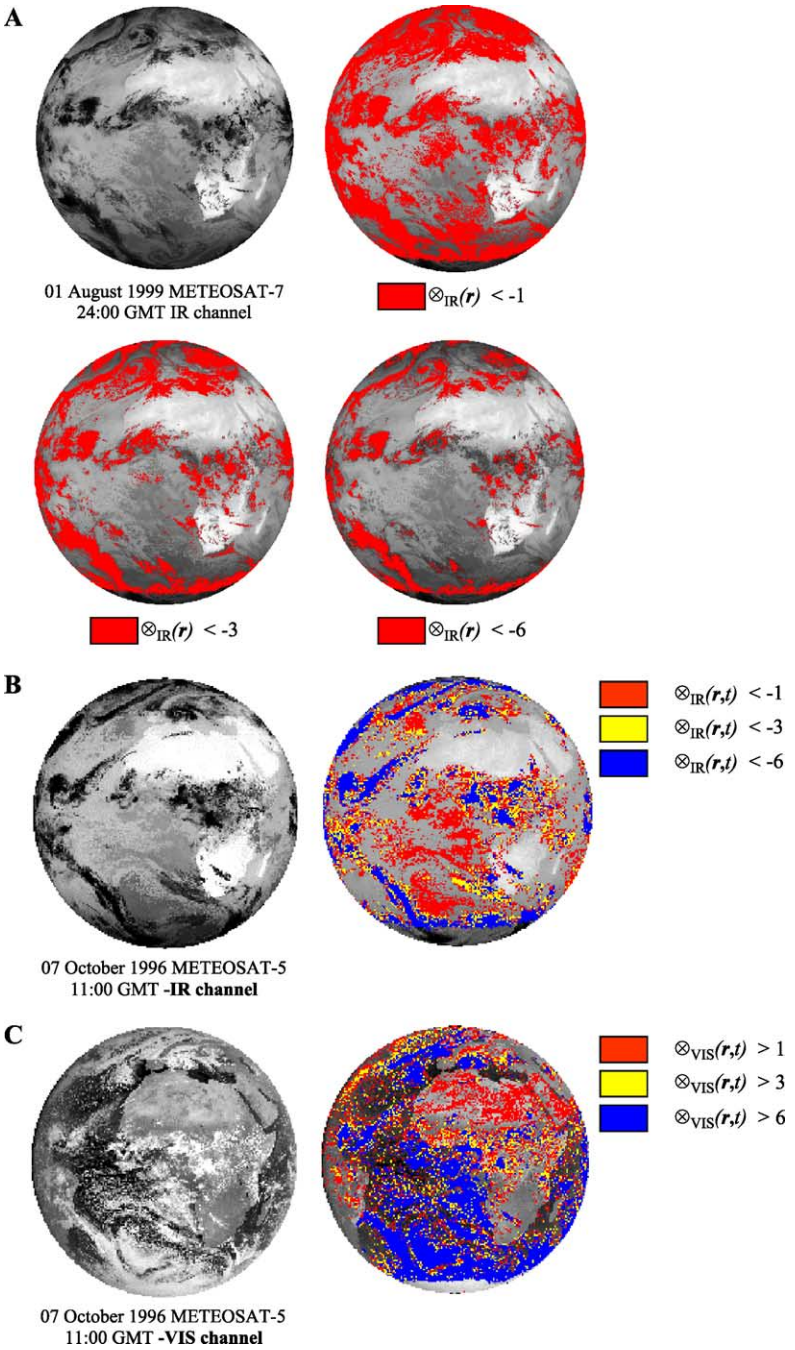

Fig. 2. Examples of cloudy radiance masks: (A) 1st August 1999, 24:00 GMT—IR channel; (B) 7th October 1996, 11:00 GMT—IR channel; (C) 7th October 1996, 11:00 GMT—VIS channel.

significantly differ from visible clear-sky radiances. Such differences among clouds, in terms of significant signal variations in a specific band, can be revealed, therefore, only by means of cloudy radiance masks because, as already underlined in Introduction, a cloud mask would indicate only the presence of all clouds, but not their effect on each single channel.

The analysis performed on several Meteosat images, selecting different cloud types and various cloud-surface contrast conditions, demonstrated OCA to have a high-detection capability. The results were confirmed by a further check performed by comparing OCA results with CLoud Analysis (CLA), the EUMETSAT operational product devoted to cloudy pixels identification. In this case, the OCA scheme was used in cloud mask mode, flagging as cloudy the pixels having $\otimes_{IR}(\boldsymbol{r},t) < -1$ or $\otimes_{VIS}(\boldsymbol{r},t) > 3$. In addition, such an analysis showed OCA sensitivity to cloud identification, with more than 95% of coincidences between OCA and CLA.

4. OCA for GERB

GERB, the broadband radiometer onboard the MSG platform, measures radiances within two ranges (Luhmann, 2002): $0.32 \div 4$ μm (*short wave*) and $0.32 \div 30$ μm (*total wave*). A *long wave* radiance, L_{lw}, is computed by means of the following equation:

$$L_{lw} = L_{tot} - A \bullet L_{sw}$$

where L_{tot} is the measured *total wave* radiance, L_{sw} is the measured *short wave* radiance, A is a constant factor (equal to 1.127) which takes the difference of time acquisition of L_{sw} and L_{tot} into account (Dewitte, 2000).

Short wave and long wave radiances contain both a solar and a thermal contribution:

$$L_{sw} = L_{sw,sol} + L_{sw,th} \text{ and } L_{lw} = L_{lw,sol} + L_{lw,th}$$

Most of the applications of satellite-based broadband radiometer measurements (ERB, meteo, etc.) needs the splitting of the energy leaving the Earth into solar and thermal contributions. For this reason, henceforth we will deal with GERB radiances not in terms of long and short wave radiances but in terms of the solar and thermal ones, being related each other in this way:

$$L_{sol} = \alpha L_{sw} \text{ and } L_{th} = \beta L_{lw}$$

where α and β are two factors which can be estimated by spectral modelling (see Clerbaux and Dewitte, 1999, for more details).

Since real GERB radiances are not yet available, Meteosat-7 data has been used in order to simulate GERB solar and thermal radiances (according to Clerbaux and Dewitte, 1999). GERB synthetic data has been obtained by means of a spatial (by averaging Meteosat-7 data in a 10×10 or 20×20 pixel box, according to GERB and Meteosat spatial resolution in infrared and visible channels) and spectral simulation (spectral modelling, by which Meteosat narrow bands are converted into GERB broadband radiances). In particular, according to Clerbaux and Dewitte's, (1999) equations, GERB

synthetic thermal radiances have been obtained combining Meteosat-7 Infrared (IR) and Water Vapor (WV) channels as follows:

$$L_{\mathrm{th}} = 21.56 + 19.24L_{\mathrm{wv}} + 3.45L_{\mathrm{ir}}$$

and GERB synthetic solar radiances, by using only Meteosat-7 visible images (VIS), according to the following equation:

$$L_{\mathrm{sol}} = 25.06 + 1.57L_{\mathrm{vis}}$$

Starting from IR, WV and VIS Meteosat-7 images acquired from 1998 to 2000, different data sets have been computed for thermal and solar synthetic GERB radiances.

The same processing described above in the case of Meteosat imagery has been followed for each GERB data set (composed by about 90 GERB synthetic images), in order to obtain GERB reference fields for the thermal $\otimes_{\mathrm{TH}}(\boldsymbol{r},t)$ and solar $\otimes_{\mathrm{SOL}}(\boldsymbol{r},t)$ part of the e.m. spectrum. Also in this case, a 2σ-clipping procedure has been used in order to avoid that mostly cloudy conditions dominate the averaging processes.

Fig. 3 gives just one example of GERB thermal ($\mu_{\mathrm{th}}(\boldsymbol{r})$ and $\sigma_{\mathrm{th}}(\boldsymbol{r})$) and solar ($\mu_{\mathrm{sol}}(\boldsymbol{r})$ and $\sigma_{\mathrm{sol}}(\boldsymbol{r})$) radiance reference fields obtained for the data set corresponding to the October month and to the 11:00–11:30 GMT time-slot.

Fig. 4a shows an example of a self-sufficient cloudy radiance mask obtained for the GERB synthetic thermal image of 16th October 1999, by using the weaker cut-level ($\otimes_{\mathrm{th}}(\boldsymbol{r},t) < -1$) which is the most selective for clear-radiance detection.

In order to demonstrate the differences with a co-located product, derived from a higher spatial resolution sensor, the self-sufficient GERB cloudy radiance mask has been compared to the one achievable by using a Meteosat-derived cloudy radiance mask, $\mathrm{CM_M}(i,j)$ giving for each GERB IFOV (at GERB image coordinates i,j) the fraction of cloudy Meteosat radiances within it.

Meteosat IR-cloudy radiance masks were computed using the OCA approach and the corresponding GERB cloudy radiance mask, computed on the basis of the percentage, $\mathrm{CM_M}(i,j)$, of Meteosat cloudy radiances within each GERB IFOV (at coordinates i,j), using different $\mathrm{CM_{MAX}}$ thresholds.

Fig. 4b–f show such Meteosat-derived products obtained by flagging as cloudy GERB IFOVs having $\mathrm{CM_M}(i,j) > \mathrm{CM_{MAX}}$. In this way, Fig. 4b (corresponding to $\mathrm{CM_{MAX}} = 0\%$) represents the (Meteosat-derived) GERB cloudy radiance mask which is better protected from the introduction of undesired cloud contaminated radiances. On the other hand (Fig. 4c–f), the choice of higher $\mathrm{CM_{MAX}}$ thresholds (which means to accept greater levels of cloud-contamination) permits to increase the number of clear-flagged GERB IFOVs. For $\mathrm{CM_{MAX}}$ thresholds equal to 25% (Fig. 4c), 50% (Fig. 4d), 75% (Fig. 4e) and 100% (Fig. 4f), 43%, 54%, 64% and 79% of GERB IFOVs are, respectively, flagged as clear.

In order to obtain a percentage (about 57%) of clear GERB IFOVs comparable to the one achieved by using the self-sufficient approach (Fig. 4a), more than 50% of cloud-contamination ($\mathrm{CM_{MAX}} > 50\%$) should be accepted when the co-location of a higher spatial resolution product is, instead, used (Fig. 4b–f).

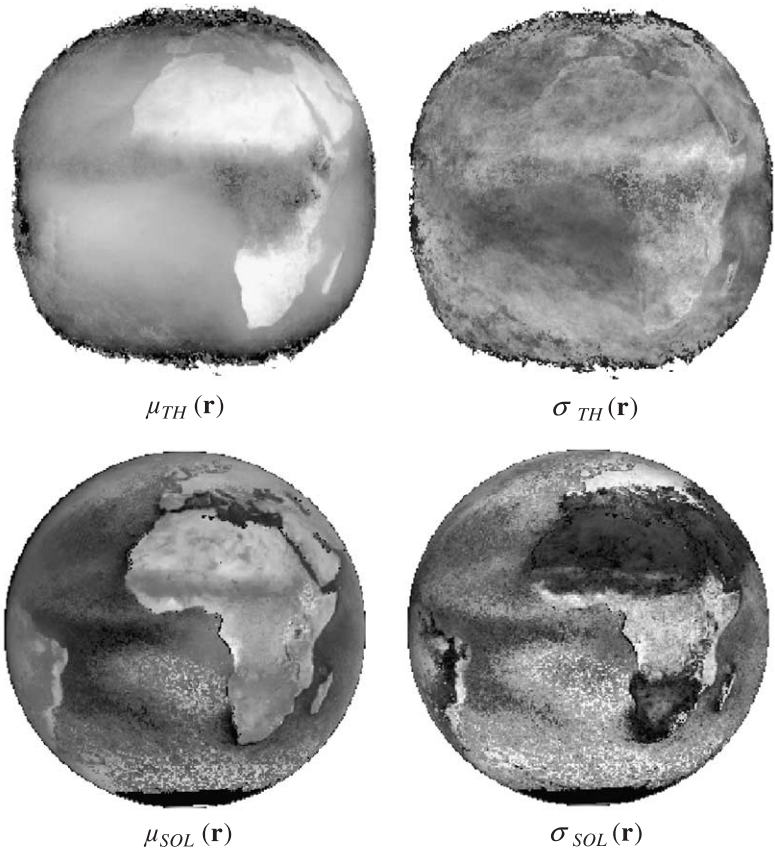

Fig. 3. Reference fields (mean and standard deviation) for GERB synthetic thermal (top) and solar (bottom) radiances, computed considering the month of October, at 11:00 GMT, from 1998 to 2000.

On the other hand, only 21% of GERB IFOVs (less than half of the ones obtained by using the proposed approach) are identified as clear when a more effective protection ($CM_{MAX}=0\%$) against cloud contamination is chosen.

Note that also the spatial distribution of clear GERB IFOVs through the scene is more homogeneous in Fig. 4a (self-sufficient approach) offering clear GERB soundings even in areas (see for example, the Eastern Africa) which appear quite overcast in the Meteosat-derived products (Fig. 4b). The doubling of clear GERB IFOVs as well as their more homogeneous distribution through the scene have been confirmed by the analysis of many images belonging to the used data set (1998–2000). How strategic these aspects are for ERB products (like cloud radiative forcing estimate) requiring an accurate reconstruction of cloud-cleared GERB radiance fields has been already explained in Introduction.

It should be noted that the effects we have just described depend only on the different spatial resolution of the considered (GERB synthetic and Meteosat) sensors. In fact, in

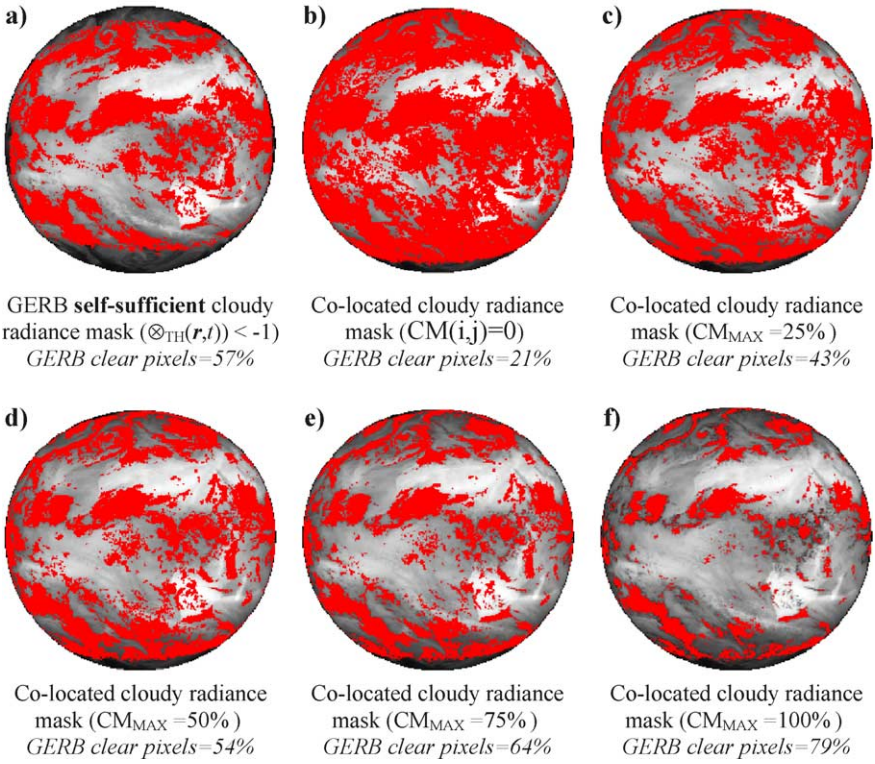

Fig. 4. Cloudy radiance masks for GERB thermal radiances of 16th October 1999. (a) GERB self-sufficient cloudy radiance mask obtained by using OCA scheme ($\otimes_{TH}(r,t)) < -1$); cloudy radiance masks for GERB images obtained by using a co-location approach: a GERB pixel is flagged as clear if it contains zero (b), less than 25% (c), 50% (d), 75% (e), 100% (f) Meteosat IR-cloudy pixels (see text). The corresponding percentage of clear-flagged GERB pixels is indicated, too.

both cases *cloudy radiance masks*—i.e. based on only one spectral band and on the same (OCA) cloudy radiance detection method—have been considered. If a *cloud mask*—derived from a sensor having not only higher spatial resolution but multi-spectral capabilities too—is used to identify (as in the case of SEVIRI for GERB) GERB cloudy radiances, worse results have to be expected. In fact, the multi-spectral information coming from the higher resolution sensor produces a cloud mask which may reveal the presence of clouds even when the radiometer does record no significant signal variations in a specific observation band. In such a case, as already said in Introduction, a further bias to a high amount of cloudy soundings has to be expected.

5. Conclusions

In order to evaluate, on the basis of GERB data, the impact of clouds on ERB, a preliminary identification of cloudy GERB radiances is required that, at present, is planned

to be provided by SEVIRI, the higher spatial and spectral resolution imager onboard the same MSG platform.

In this paper, a self-sufficient (only based on GERB data) method (OCA, the One-channel Cloudy-radiance-detection Approach) is proposed as a time-saving, and probably more reliable, alternative to the planned co-location approach.

Preliminary results obtained by using several years of Meteosat data as well as GERB synthetic radiances (produced from Meteosat-7 observations) are presented. It is shown that using the OCA approach on GERB data alone permits to identify twice cloud-free GERB pixels identified by using the co-location of a higher resolution cloud mask.

The OCA approach showed to protect, besides a greater number, a more homogeneous spatial distribution, of clear GERB soundings. This is particularly important when sensors, like GERB, are employed in ERB calculations (like cloud radiative forcing) requiring accurate reconstruction of cloud cleared radiances. Finally, it should be noted that OCA clear sky reference images themselves might represent a valid support to fill gaps left at the end of cloud-clearing processes and, due also to the very coarse GERB spatial resolution which makes not rare this circumstance, a suitable alternative to spatial interpolation where available clear-sky soundings are too few or too far from the area where cloud-cleared radiances have to be estimated.

Acknowledgements

This work has been funded by the Italian Space Agency in the framework of "GERB" project.

References

Ackerman, S.A., Strabala, K.I., Menzel, W.P., Frey, R.A., Moeller, C.C., Gumley, L.I., 1998. Discriminating clear-sky from clouds with MODIS. J. Geophys. Res. 103 (D24), 32141–32158.

Arking, A., Childs, J.D., 1985. Retrieval of cloud cover parameters from multispectral satellite measurements. J. Climate Appl. Meteor. 24, 322–333.

Clerbaux, N., Dewitte, S., 1999. RGP-SP: Spectral Modelling. RMIB technical report. MSG-RMIB-GE-TN-0005, available on the web site http://gerb.oma.be/.

Coakley, J.A., Bretherton, F.P., 1982. Cloud cover from high-resolution scanner data: detecting and allowing for partially filled fields of view. J. Geophys. Res. 87, 4917–4932.

Cressie, N.A.C., 1993. Statistics for Spatial Data. J. Wiley and Sons, Indianapolis, IN, USA.

Cuomo, V., Amato, U., Rizzi, R., Serio, C., Tramutoli, V., 1993. Topics in optimal inversion schemes applied to atmospheric structure retrieval in high spectral resolution infrared remote sensing for earth's weather and climate studies. In: Chedin, A., Chahine, M.T., Scott, N.A. (Eds.), NATO ASI Series. Series I, Global Environmental Change, vol. 9. Springer-Verlag, Berlin, pp. 163–174.

Cuomo, V., Tramutoli, V., Pergola, N., Pietrapertosa, C., Romano, F., 1997. In place merging of satellite based atmospheric water vapor measurements. Int. J. Rem. Sens. 18 (17), 3649–3668.

Cuomo, V., Pietrapertosa, C., Serio, C., Tramutoli, V., 1999. Assessing the impact of cloud morphology on infrared scan geometry. Int. J. Rem. Sens. 20 (1), 169–181.

Cuomo, V., Lasaponara, R., Tramutoli, V., 2001. Evaluation of a new satellite-based method for forest fire detection. Int. J. Rem. Sens. 22 (9), 1799–1826.

Derrien, M., Farki, B., Harang, L., Le Gleau, H., Noyalet, A., Pochic, D., Sairouni, A., 1993. Automatic cloud detection applied to NOAA-11/AVHRR imagery. Rem. Sens. Envir. 46, 246–267.

Dewitte, S., 2000. RGP: data products accuracy estimation. RMIB technical report. MSG-RMIB-GE-TN-0011, available on the web site http://gerb.omabe/.

Di Bello, G., Filizzola, C., Lacava, T., Marchese, F., Pergola, N., Pietrapertosa, C., Piscitelli, S., Scaffidi, I., Tramutoli, V., 2004. Robust satellite techniques for volcanic and seismic hazards monitoring. Ann. Geoph. 47 (1), 13–24.

Filizzola, C., Pergola, N., Pietrapertosa, C., Tramutoli, V., 2004. Robust satellite techniques for seismically active areas monitoring: a sensitivity analysis on September 7th 1999 Athens's earthquake. Phys. Chem. Earth 29, 517–527.

Gutman, G., Ignatov, A., Olson, S., 1994. Towards better quality of AVHRR composite imagers over land: reduction of cloud contamination. Rem. Sens. Envir. 50, 134–148.

Gutman, G., Ignatov, A., Olson, S., 1996. Global land monitoring using AVHRR time series. Adv. Space Res. 17, 151–154.

Lasaponara, R., Tramutoli, V., Cuomo, V., 1998. Fire-detection by AVHRR: toward a new generalized approach for operational monitoring. In: Engman, E.T. (Ed.), Remote Sensing for Agriculture, Ecosystems, and Hydrology. Proceedings of SPIE the International Society for Optical Engineering, P.O. Box 10, Bellingham, Washington 98227-0010, USA, vol. 3499, pp. 348–358.

Luhmann, H.J., 2002. MSG's GERB Instrument. ESA Bulletin 111, 18–20 (August), available on the website http://esapub.esrin.esa.it.

Menke, W., 1984. Geographical data analysis: discrete inverse theory. Academic Press, New York.

Pergola, N., Tramutoli, V., 2000. SANA: Sub-pixel Automatic Navigation of AVHRR imagery. Int. J. Rem. Sens. 21 (1), 2519–2524.

Pergola, N., Tramutoli, V., 2003. Two years of operational use of SANA (Sub-pixel Automatic Navigation of AVHRR) scheme: accuracy assessment and validation. Rem. Sen. Envir. 82 (2), 190–203.

Pergola, N., Tramutoli, V., Pietrapertosa, C., 1998. Satellite remote sensing of volcanic aerosols: a new, AVHRR-based, approach. In: Russel, J.E. (Ed.), Satellite Remote Sensing of Clouds and the Atmosphere III. Proceedings of SPIE the International Society for Optical Engineering, P.O. Box 10, Bellingham, Washington 98227-0010, USA, vol. 3495, pp. 188–197.

Pergola, N., Pietrapertosa, C., Lacava, T., Tramutoli, V., 2001. Robust satellite techniques for monitoring volcanic eruptions. Ann. Geoph. 44 (2), 167–177.

Pergola, V., Tramutoli, I., Scaffidi, T., Lacava, F., Marchese, 2004. Improving volcanic ash clouds detection by a robust satellite technique. Rem. Sens. Envir. 90 (1), 1–22.

Pietrapertosa, C., Cuomo, V., Pergola, N., Serio, C., Tramutoli, V., Shimoda, H., 2001a. Fractality in broken clouds and the scan geometry of new satellite-borne infrared sensors. Int. J. Rem. Sens. 22 (5), 889–894.

Pietrapertosa, C., Pergola, N., Lanorte, V., Tramutoli, V., 2001b. Self adaptive algorithms for change detection: OCA (the One-channel Cloud-detection Approach) an adjustable method for cloudy and clear radiances detection. In: Le Marshall, J.F., Jasper, J.D. (Eds.), Technical Proceedings of the Eleventh International (A)TOVS Study conference (ITSC-XI) Budapest, Hungary, 20–26 September 2000. Bureau of Meteorology Research Centre, Melbourne, Australia, pp. 281–291.

Rizzi, R., Serio, C., Kelly, G., McNally, A., Tramutoli, V., Cuomo, V., 1994. Cloud clearing of infrared sounder radiances. J. App. Meteorology 33 (2), 180–194.

Rossow, W.B., Garder, L.C., 1993. Cloud detection using satellite measurements of infrared and visible radiances for ISCCP. J. Climate 2, 419–458.

Saunders, R.W., 1986. An automated scheme for the removal of cloud contamination from AVHRR radiances over western Europe. Int. J. Rem. Sens. 7, 867–886.

Saunders, R.W., Kriebel, K.T., 1988. An improved method for detecting clear sky and cloudy radiances from AVHRR data. Int. J. Rem. Sens. 9, 123–150.

Serio, C., Tramutoli, V., 1995. Scaling laws in a turbulent baroclinic instability. Fractals 3 (2), 297–314.

Stowe, L.L., McClain, E.P., Carey, R., Pellegrino, P., Gutman, G., Davis, P., Long, C., Hart, S., 1991. Global distribution of cloud cover derived from NOAA/AVHRR operational satellite data. Adv. Space Res. 11, 51–54.

Stowe, L.L., Davis, P.A., McClain, E.P., 1999. Scientific basis and initial evaluation of the CLAVR-1 global clear/cloud classification algorithm for the advanced very high resolution radiometer. J. Atmos. Oceanic Technol. 16, 656–681.

Tramutoli, V., 1998. Robust AVHRR Techniques (RAT) for environmental monitoring: theory and applications. In: Giovanna, C., Eugenio, Z. (Eds.), Earth Surface Remote Sensing II. Proceedings of SPIE the International Society for Optical Engineering, P.O. Box 10, Bellingham, Washington 98227-0010, USA, vol. 3496, pp. 101–113.

Tramutoli, V., Pietrapertosa, C., Lanorte, V., 1998. Clouds spatial distribution and infrared sounding contamination: an impact study on infrared satellite sounding of the atmosphere. In: Eyre, J.R. (Ed.), Technical Proceedings of the Ninth International TOVS Study Conference, Igls, Austria. ECMWF, Reading, pp. 487–498.

Tramutoli, V., Lanorte, V., Pergola, N., Pietrapertosa, C., Ricciarelli, E., Romano, F., 2000. Self-adaptive algorithms for environmental monitoring by SEVIRI and GERB: a preliminary study. Proceedings of EUMETSAT Meteorological Satellite Data Users' Conference, Bologna (Italy), 79–87.

Tramutoli, V., Di Bello, G., Pergola, N., Piscitelli, S., 2001a. Robust satellite techniques for remote sensing of seismically active areas. Annals of Geophysics 44 (2), 295–312.

Tramutoli, V., Pergola, N., Pietrapertosa, C., 2001b. Training on NOAA-AVHRR of robust satellite techniques for next generation of weather satellites: an application to the study of space–time evolution of Pinatubo's stratospheric volcanic cloud over Europe. In: Smith, W.L., Timofeyev, Yu.M. (Eds.), IRS 2000: Current Problems in Atmospheric Radiation. A. Deepak Publishing, Hampton, VA, pp. 36–39.

Vemury, S., Stowe, L.L., Anne, V.R., 2001. AVHRR pixel level clear-sky classification using dynamic thresholds (CLAVR-3). J. Atmos. and Oceanic Technology 18, 169–186.